Facile synthesis of nanosheet-assembled -Fe2O3 magnetic microspheres and enhanced Sb(III) removal

Zhao, Wenlin; Ren, Bozhi; Hursthouse, Andrew; Wang, Zhenghua

Published in:
Environmental Science and Pollution Research

DOI:
10.1007/s11356-020-11727-7

Published: 06/01/2021

Document Version
Peer reviewed version

Facile synthesis of nanosheet-assembled -Fe2O3 magnetic microspheres and enhanced Sb(III) removal

Zhao, Wenlin; Ren, Bozhi; Hursthouse, Andrew; Wang, Zhenghua

Published in:
Environmental Science and Pollution Research

DOI:
10.1007/s11356-020-11727-7

Published: 06/01/2021

Document Version
Peer reviewed version

Environ Sci Pollut Res (2021)
https://doi.org/10.1007/s11356-020-11727-7

Facile synthesis of nanosheet-assembled γ-Fe_2O_3 magnetic microspheres and enhanced Sb(III) removal

Wenlin Zhao[1,2], Bozhi Ren [1,2,*], Andrew Hursthouse [1,3], Zhenghua Wang[1,2]

[1] School of Civil Engineering, Hunan University of Science and Technology, Xiangtan, 411201, China; E-Mails: 18020201021@mail.hnust.edu.cn (W.Z.); BozhiRen@126.com (B.R.); andrew.hursthouse@uws.ac.uk (A.H.); wzh@hnust.edu.cn (Z.W.);

[2] Hunan Provincial Key Laboratory of Shale Gas Resource Exploitation, Xiangtan, 411201, China;

[3] Computing Engineering & Physical Sciences, University of the West of Scotland, Paisley PA1 2BE, UK;

* Corresponding author: BozhiRen@126.com (B.R.); Tel. +86-13107126636; Fax: +86-0731-58290182

Abstract

The development and utilization of magnetic nano adsorption materials with large adsorption capacity and easy separation are the research hotspot nowadays. In this study, nanosheet-assembled maghemite (γ-Fe_2O_3) magnetic microspheres were successfully synthesized by an environmental friendly, quick and simple method, for enhanced Sb(III) removal from aqueous solution. Scanning electron microscopy (SEM), X-ray diffraction (XRD), X-ray photoelectron spectroscopy (XPS), vibrating sample magnetometer (VSM), and Brunauer-Emmett-Teller (BET) were used to characterize the material. The results showed that the product contained flower-like γ-Fe_2O_3 microspheres composed of petal-shaped nanosheets interspersed with each other. The specific surface area and pore volume were 69.23 m^2/g and 0.15 cm^3/g, respectively. The material has a strong magnetic response, which allows rapid solid-liquid

separation under the action of an external magnetic field. The effects of different dosages, solution pH and contact time on the adsorption effect were studied by batch adsorption experiments, and the reusability of the materials was evaluated. Both Freundlich isothermal adsorption model and pseudo-second order kinetic model were able to describe the uptake of Sb(III). The maximum adsorption capacity of the material was 47.48 mg/g under optimal conditions. The adsorption mechanism is mainly that Sb and lattice oxygen (O_X^{2-}) form Fe-O-Sb coordination bonds, which is incorporated into the crystal structure of γ-Fe_2O_3 as inner-sphere surface complexes. The synthetic material has the advantage of simple preparation process, good adsorption capacity, operation over a wide range of pH, and easy physical separation from treatment systems with good potential for future application to treat polluted waste water.

Keywords Antimony Wastewater · Nanomaterials · Iron oxide · Magnetic microspheres · Adsorption performance

Introduction

Antimony is a silver-white metal, and its compounds are important raw materials for products such as flame retardants, alloys, and emerging microelectronic technology(He et al. 2019, Zhou et al. 2018). In recent decades, the global demand for and subsequent extraction of antimony from ores has caused antimony to enter and pollute the water environment (Li et al. 2018a, Ren et al. 2016, Telford et al. 2009). In aqueous solution antimony is predominantly in the form of Sb(III) and Sb(V) with, Sb(III) being ten times more biotoxic than Sb(V). Antimony poisoning can cause severe damage to the mucous membranes, heart, liver, lungs and nervous system, and it is a potential carcinogen (Ren et al. 2018, Ren et al. 2019). At present, the removal techniques of heavy metal antimony mainly include adsorption(Guo et al. 2014), coagulation precipitation(Guo et al. 2018), membrane separation(Nishiyama et al. 2003), biological method(Zhang et al. 2016), etc. Among those methods, adsorption has attracted widespread attention as

47 an efficient and economic method for water treatment (Ungureanu et al. 2015).

48 In recent years, iron-based composite materials have been widely used in lithium-ion batteries,
49 catalysts, sensors, and adsorption materials(Fiore et al. 2018, Sun et al. 2016). Among them, magnetic
50 iron oxides (Fe_3O_4, γ-Fe_2O_3) has superparamagnetic property, when they are used as adsorbents for water
51 treatment, they can be quickly separated from water treatment under the action of an external magnetic
52 field(Patra et al. 2019). At the same time, the development of nanotechnology has made nanomaterials
53 widely used in environmental restoration and treatment of water pollution (Gusain et al. 2020). In
54 particular, three-dimensional (3D) microspheres self-assembled nano-structure units have a large specific
55 surface area, using it for adsorption materials can provide a large number of active adsorption
56 sites(Khosravi and Azizian 2014). Therefore, the introduction of nanoscale to magnetic iron oxide-based
57 adsorption materials will greatly increase its removal efficiency of pollutants and have the advantages of
58 easy separation and recycling. However, although there have been many studies using iron oxide to
59 remove potentially toxic elements (Ma et al. 2018, Ramirez-Muñiz et al. 2012), there are few reports on
60 the use of maghemite to remove Sb(III). In summary, the development of a magnetic 3D nanostructured
61 microspheres has potentially very important practical application in cleaning the water environment.

62 At present, the main methods for laboratory synthesis of iron oxide include hydrothermal or
63 solvothermal technique(Tadic et al. 2019), co-precipitation method(Piraman et al. 2016), sol-gel
64 process(Niu et al. 2018), and template-directed synthetic route(Wang and Lo 2009). But these methods
65 have the disadvantage of harsh synthesis conditions, long time-consuming preparation, and relatively
66 high cost. Recently, the preparation of 3D iron oxide with a specific morphology was described
67 synthesized by calcining iron alkoxide precursors formed by an ethylene glycol (EG)-mediated self-
68 assembly process(Sun et al. 2016). Penki et al.(Penki et al. 2015) used ferric chloride hexahydrate ($FeCl_3$

• $6H_2O$) and urea as raw materials to obtain ferric alkoxide precursor by a reflux method at 195° C for 30 min with the aid of surfactant tetrabutylammonium bromide (TBAB), then calcined it at high temperature to successfully synthesize α-Fe_2O_3. Zhong's team(Zhong et al. 2006) used the same chemical agent to successfully synthesize α-Fe_2O_3, γ-Fe_2O_3, and Fe_2O_3 with 3D nanostructures by controlling reflux and calcining conditions. In the absence of surfactants, Liu et al.(Liu et al. 2015) used ferrous chloride tetrahydrate($FeCl_3$ • $4H_2O$) and urea as raw materials by solvothermal treatment at 160 ℃ for 12 h to synthesize superparamagnetic Fe_3O_4@(α-γ)-Fe_2O_3 watercress. Ma's group(Ma et al. 2013) dissolved ferric acetylacetonate ($Fe(acac)_3$) in ethylene glycol solution, and continuously stirred in an oil bath at 160 ℃ for 3 h to successfully prepare the ferric alkoxide precursor, which was then converted into flower-like and yarn-like α-Fe_2O_3 spherical clusters by calcination at high temperature.

In this study, a facile method was used to synthesize γ-Fe_2O_3 magnetic microspheres formed by self-assembly of nanosheets structures for enhanced Sb(III) removal from aqueous solutions. First, the iron alkoxide precursor was synthesized under microwave-assisted conditions, using non-toxic and inexpensive source of iron (iron chloride, $FeCl_3$ • $6H_2O$), urea and ethylene glycol as raw materials. The reason for adding urea is that the OH^- produced by its hydrolysis can neutralize the large amount of HCl produced during the reaction(Zhong et al. 2006), making the reaction proceed in a forward direction. Then, the iron alkoxide precursor was calcined in an air atmosphere at a certain temperature to synthesize nanosheet-assembled γ-Fe_2O_3 magnetic microspheres. The material was characterized using SEM, XRD, XPS and VSM. The adsorption performance of the product was studied by conducting batch adsorption experiments to study the effects of dose, pH, contact time, adsorption thermodynamics and adsorption kinetics, to assess the practical application potential of this adsorbent.

Materials and Methods

Materials

All chemicals used in this study were of analytical grade and were not further purified before use. All solutions were prepared with deionized water. Ferric trichloride ($FeCl_3 \cdot 6H_2O$), urea [$CO(NH_2)_2$], Ethylene glycol [$(CH_2OH)_2$], potassium antimony tartrate ($C_8H_4K_2O_{12}Sb_2$) were purchased from Sinopharm Chemical Reagent Co., Ltd. (China, Shanghai). Absolute ethanol (C_2H_5OH), hydrochloric acid (HCl) and sodium hydroxide (NaOH) were purchased from XiLong Science Co., Ltd. (Shantou, China).

Preparation of nanosheet-assembled maghemite magnetic microspheres

First, 2 mol (0.5406 g) of $FeCl_3 \cdot 6H_2O$ and 6 mol (0.3603 g) of urea were added in a polytetrafluoroethylene reaction tank containing 35 mL of ethylene glycol solution under magnetic stirring. After stirring for 30 minutes, a homogeneous transparent red solution was obtained, the solution was subsequently transferred to a microwave-hydrothermal synthesis system (MDS-6, Sineo, China) at 60 % power for 20 minutes, a pale green precipitate was formed. The precipitate was collected and repeatedly washed with alcohol and deionized water, centrifuged, and then dried overnight in a vacuum oven at 60 ℃, the product obtained was the iron alkoxide precursor. Finally, the dried precursor was moved into a program-controlled temperature furnace (KSL-1100X, Dehui, China) and calcined at 300 ℃ for 1 h. After cooling to room temperature, a red-brown powder was obtained, which was the target product. The schematic diagram of the synthesis process is shown in Fig. 1.

Characterizations

The surface morphology of the fresh product and after adsorption reaction were studied using field emission scanning electron microscope (SEM, Hitachi S4800, Japan) which also equipped with an

112 energy dispersive spectroscope. An X-ray diffractometer (Rigaku smartlab-9, Japan) was used to collect
113 the X-ray diffraction (XRD) pattern of the product. X-ray photoelectron spectroscopy (XPS) of the
114 product before and after adsorption experiments was collected by an X-ray photoelectron spectrometer
115 (Thermo Fisher Scientific EscaLab 250Xi, USA) for qualitative analysis of its elemental composition.
116 The magnetic response of the product was assessed by a vibration sample magnetometer (VSM,
117 Microsecse EZ9, USA). The isothermal adsorption-desorption curve for nitrogen was obtained by a
118 porous physical adsorber (Quantachrome Autosorb EVO, USA). The Brunauer-Emmett-Teller (BET)
119 and the Barrett-Joyner-Halenda (BJH) methods were used to determine the specific surface area and pore
120 size distribution.

121 **Batch adsorption experiment**

122 A batch adsorption experiment was performed to determine the optimal conditions for the removal
123 of Sb(III) from the aqueous solution and to evaluate the adsorption performance of nanosheet-assembled
124 γ-Fe_2O_3 magnetic microspheres. A stock solution (200mg/L) of Sb(III) was prepared from antimony
125 potassium tartrate dissolved in deionized water and stored in dark. In subsequent experiments, Sb(III)
126 solution with different concentrations were prepared by diluting the stock solution in a certain proportion.
127 Tests were undertaken using 100 mL of Sb(III) solution in a 250 mL conical flask, the effect of pH on
128 the sorption capacity of the γ-Fe_2O_3 magnetic microspheres was investigated in a pH range from 1.0 to
129 11.0, in addition, the effect of adsorbent dose and contact time on the adsorption efficiency were also
130 carried out by the same procedure. The initial pH of the solution is adjusted by HCl and NaOH solutions
131 (0.1M) and recorded with a pH meter (PB10, Sartorius, Germany) before the addition of sorbent. Then,
132 a portion of adsorbent (50~300 mg) was added and transferred to an oscillating incubator (150 rpm) for
133 reaction under different temperature conditions (25~45℃). After reaction the adsorbent was separated

from the solution using a magnet, a 10 mL portion of the supernatant was take out and filtered using a 0.45 μm pore size membrane filter, and the concentration of Sb(III) remaining in the solution after adsorption was determined by an atomic absorption spectrometer (AA-7050, ewai, China). The removal rate R(%) of Sb(III) and the adsorption capacity (qt, qe (mg/g)) at any time t of the adsorption reaction and the equilibrium of the adsorption in the adsorption experiments of each group were calculated with the equations below:

$$R(\%) = \frac{C_0 - C_e}{C_0} \times 100 \quad (1)$$

$$q_t = \frac{(C_0 - C_t) \cdot V}{m} \quad (2)$$

$$q_e = \frac{(C_0 - C_e) \cdot V}{m} \quad (3)$$

Where C_0, C_e, and C_t represents the concentration (mg/L) of Sb(III) in the solution at the initial, equilibrium and any time, respectively; V is the volume (L) of Sb(III) solution and m is the weight of dry adsorbent (g). All experimental data used were averaged over three repetitions experiments.

The pseudo-first order kinetic (Eq. 4) and pseudo-second order kinetic (Eq. 5) models were used to analyze the adsorption process. The specific mathematical equations are as follows:

$$ln(q_e - q_t) = lnq_e - k_1 t \quad (4)$$

$$\frac{t}{q_t} = \frac{1}{k_2 {q_e}^2} + \frac{t}{q_e} \quad (5)$$

Where k_1 and k_2 are the adsorption rate constants of the pseudo-first order kinetic and the pseudo-second order kinetic, respectively.

Langmuir (Eq. 6) and Freundlich (Eq. 7) isotherm adsorption models were used to fit the experimental data. the specific formulas are as follows:

$$q_c = \frac{Q_0 K_L C_e}{1 + K_L C_e} \quad (6)$$

$$q_c = K_F {C_e}^{1/n} \quad (7)$$

Where q_c is the equilibrium adsorption capacity value (mg/g); C_e is the equilibrium concentration

(mg/L); Q_0 is the saturated adsorption capacity (mg/g); K_L is the adsorption coefficient, and its value is related to the temperature and the nature of the adsorbent and the adsorbent; K_F and 1/n are parameters related to adsorption capacity and adsorption strength in the Freundlich model.

The Gibbs free energy change (ΔG^0), standard enthalpy change (ΔH^0) and entropy change (ΔS^0) were calculated by the following equations:

$$K_T = \frac{q_e}{C_e} \quad (8)$$

$$\ln K_T = \frac{\Delta S^0}{R} - \frac{\Delta H^0}{RT} \quad (9)$$

$$\Delta G^0 = \Delta H^0 - T\Delta S^0 \quad (10)$$

Where K_T (L/g) is the adsorption equilibrium constant, R (8.314 kJ/mol) is the universal gas constant and T is the absolute temperature in Kelvin.

Results and discussion

Characterization of the synthetic material

SEM-EDS analysis

Fig. 2(a~e) shows scanning electron microscope images of the product, and Fig. 2(f) is a scanning electron microscope image after the product adsorbs Sb(III). As shown in Fig. 2(c) and (d), the product is a flower-like 3D microspheres with a particle size of about 4 μm, which is composed of overlapping and interspersing petal-shaped nanosheets about 30 nm thick. A large number of pores exist on the surface, which enhances contact between the target pollutant and the material, and can provide a large number of adsorption sites. Comparing Fig. 2(e) and (f), it can be seen that after the adsorption reaction occurs, a large amount of amorphous granules are attached to the surface of the material. It is speculated that this is due to the drying process after adsorption, causing the Sb(III) adsorbed on the surface of the material to be oxidized, and thus adheres to the product surface as an amorphous solid granule. Additionally, EDS results confirmed that the product mainly contains O and Fe two elements; while the occurrence of

Sb element after adsorption, confirmed that Sb(III) was adsorbed onto the surface of the product.

XRD and XPS analysis

Fig. 3 shows the X-ray diffraction pattern of the product synthesized by two-step method. It can be seen from the figure that the positions and relative intensities of all diffraction peaks of the product are matched with γ-Fe_2O_3 (JCPDS#39-1346) and Fe_3O_4 (JCPDS#88-0315). However, since both have very similar lattice structure parameters, XRD cannot completely distinguish the two, so it is necessary to continue to use other characterization methods for testing and analysis(Qi et al. 2017). The high-resolution curve-fitted XPS spectrum of Fe2p is shown in Fig. 4. The peaks at the binding energy of 711.36eV and 724.46eV are consistent with the binding energy of Fe 2p1/2 and Fe 2p3/2 orbits of γ-Fe_2O_3, respectively(Torkashvand and Sarlak 2019). At the same time, the appearance of the satellite peak at 720eV further confirmed that the product synthesized was γ-Fe_2O_3(Yamashita and Hayes 2008).

Fig. 5 shows The XPS survey spectra of full scan of γ-Fe_2O_3 magnetic microspheres after Sb(III) adsorption (Fig. 5a), high-resolution O 1s spectrum before adsorption (Fig. 5b), high-resolution O 1s+Sb 3d spectrum after adsorption (Fig. 5c), and high-resolution of Fe 2p spectrum before and after adsorption (Fig. 5d), respectively. The appearance of the characteristic peak of Sb 3d binding energy in the full scan spectrum shows that γ-Fe_2O_3 interacts with Sb(III), thereby effectively transferring Sb(III) from solution to γ-Fe_2O_3 magnetic microspheres. The binding energy peaks of 529.86eV and 539.71eV in Fig. 5c correspond to the positions of the standard binding energy peaks of Sb 3d5/2 and Sb 3d3/2, respectively. Studies have shown that the valence states of these two peaks corresponding to Sb include Sb(V) And Sb(III)(Li et al. 2018b). The O 1s core level region of γ-Fe_2O_3 is composed of the lattice oxygen (O_X^{2-}) and surface hydroxyl groups(-OH)(Flak et al. 2018). In Figure 5b, the separation of the O1s peak composed of Fe-O-Fe (529.58 eV) and Fe-OH (531.43 eV), respectively(Li et al. 2017). Comparing with

Fig. 5b and Fig. 5c, the binding energy peak position and area of the lattice oxygen (O_X^{2-}) have changed after adsorption, indicating that γ-Fe_2O_3 and Sb(III) underwent chemical reaction. The peak of O_X^{2-} at 529.58 eV blue shifted to 530.27, indicating that O atom donated the lone pair electrons to the vacant orbitals of Sb(III) to form coordination bond (surface complexation)(Bulin et al. 2020).In Fig. 5d, comparing the high-resolution spectra of Fe 2p before and after adsorption, it can be seen that the binding energy peaks at the orbits of Fe 2p1/2 and Fe 2p3/2 after adsorption are respectively moved from 711.36 eV and 724.46 eV to 711.15 eV and 724.25 eV before adsorption. Both of them shifted to the lower field, indicating that Fe gained electrons. On the one hand, in combination the occurrence of Sb(V) in Fig. 5c, it is speculated that it may be due to the redox reaction between γ-Fe_2O_3 and Sb(III), which caused partial electrons on Sb(III) to be transferred to Fe(III)(Qi et al. 2016); on the other hand, combining the research of Jordan N et al.(Jordan et al. 2014), Morin G et al.(Morin et al. 2008), and Kirsch R et al.(Kirsch et al. 2008), speculated the adsorption mechanism of the nanosheet-assembled γ-Fe_2O_3 magnetic microspheres is that Sb and the lattice oxygen (O_X^{2-}) form Fe-O-Sb coordination bonds through sharing electron pairs, which is incorporated into the crystal structure of γ-Fe_2O_3 as inner-sphere surface complexes.

VSM analysis

In order to test the magnetic properties of the synthesized γ-Fe_2O_3 magnetic microspheres, the magnetization hysteresis loop was characterized at room temperature (Fig. 6). As shown in Fig. 6, it can be seen from the figure that the magnetization curve of γ-Fe_2O_3 magnetic microspheres presents a symmetrical S-type, and its magnetization increases with the increase of the applied magnetic field strength, and the saturation magnetization is 52.91 emu/g, indicating that it has strong magnetic response properties. When the applied magnetic field is 0, the residual magnetization and coercivity of γ-Fe_2O_3 magnetic microspheres are also 0, which belongs to the soft magnetic category, indicating that it has

superparamagnetism(Ge et al. 2007). Materials with superparamagnetism can quickly disperse in the liquid environment without applying an external magnetic field, and there will be no agglomeration due to the magnetic interaction between the materials, which facilitates the adsorption of γ-Fe_2O_3 magnetic microspheres to avoid complex pre-processing procedures. Fig. 6 illustrates that under the action of an external magnetic field, the synthesized nanomaterials can be quickly separated from the aqueous solution, which is beneficial to the separation and recovery and reuse of the materials(Wang et al. 2015).

BET analysis

Isothermal nitrogen adsorption-desorption tests were performed on the synthesized product and the specific surface area and porosity characteristics were analyzed. The results are shown in Fig. 7 (inset is the BJH pore size distribution of synthesized γ-Fe_2O_3 microspheres). According to the classification of IUPAC, the nitrogen adsorption-desorption isotherm of γ-Fe_2O_3 microspheres is a type III isotherm, the adsorbate will clustered around the most favorable sites on the surface of the adsorbent(Thommes et al. 2015). The pore size distribution showed that there was a distribution peak of maghemite microspheres at 2 nm and 10 nm respectively. According to the Brunauer-Emmett-Teller (BET) and Barrett-Joiner-Halenda (BJH) method, the specific surface area and pore volume of synthesized γ-Fe_2O_3 magnetic microspheres are 69.23 m^2/g and 0.15 cm^3/g. It can provide and expose more adsorption sites(Li et al. 2019), making it have excellent adsorption performance of heavy metals.

Adsorption studies by batch experiments

Effect of dosage of adsorbent on Sb(III) removal

The dose of the adsorbent is an important index for controlling costs in practical applications. In order to further optimize the use of the adsorbent, γ-Fe_2O_3 magnetic microspheres with dry weights of 50, 100, 150, 200, 250, and 300 mg were used in the experiments, added to a 100 mL aqueous solution

with an initial concentration of 10 mg/L of Sb(III), control the pH of the solution to 7.0, the reaction temperature to 298.15 K, the speed of the constant temperature incubator shaker to 150 rpm, and the contact time t=240 min, to explore the effect of the amount of adsorbent on the adsorption performance of Sb(III) in aqueous solution (Fig. 8).

It can be seen from the figure that with the increase of the adsorbent dose, the removal efficiency gradually increased. When the dose was 200 mg (2g/L), the removal efficiency of Sb(III) reached 98.3%. At low doses, there were fewer adsorption sites, and there was a positive correlation between the adsorption sites and adsorption efficiency of the adsorption materials(Hao et al. 2010), which results in a low removal efficiency of Sb(III) by γ-Fe_2O_3 magnetic microspheres. With the increase of the dose, on the one hand, the adsorption sites in the solution increased rapidly, and γ-Fe_2O_3 magnetic microspheres could coordinate with more Sb(III) ions to form complexes, thus reducing the content of Sb(III) ions in the solution; on the other hand, the probability that the adsorbed substance and the adsorbent collide with each other will increase accordingly, so the removal efficiency will increase rapidly. In consideration of economic benefits, 200 mg was selected as the optimal dose in subsequent experiments.

Effect of pH

The pH value of the aqueous solution is one of the important factors affecting the adsorption process, and it has a significant effect on the form and type of metal ions and the physicochemical properties of the adsorbent(Ma et al. 2016). γ-Fe_2O_3 magnetic microspheres with a dry weight of 200 mg were added to 6 groups aqueous solutions with an initial concentration of 10 mg/L of Sb(III) in the pH range of 1.0~11.0. Controlling the reaction temperature to 298.15 K and the contact time t=240 min, study on the adsorption properties of γ-Fe_2O_3 magnetic microspheres (Fig. 9).

As shown in Fig. 9, in the pH range 3.0 to 9.0, the removal efficiency of Sb(III) by γ-Fe_2O_3 magnetic

microspheres hardly changes; when the pH was around 1.0 and 11.0, the Sb(III) The removal efficiency was slightly reduced, but the removal efficiencies were all above 90.3±0.8%, indicating that the γ-Fe_2O_3 magnetic microspheres had a wide range of adaptation to pH. The effect of pH value on the removal of Sb(III) by γ-Fe_2O_3 magnetic microspheres is not only related to the species of Sb(III) at different pH(Zhao et al. 2014), but also the charge characteristics on the surface of γ-Fe_2O_3 magnetic microspheres(Üçer et al. 2006). The pHzpc (the point of zero charge) of γ-Fe_2O_3 is 6.3(Abdullah et al. 2019). When the pH of the solution is lower than 6.3, the surface of the γ-Fe_2O_3 magnetic microspheres is positively charged. Conversely, the surface is negatively charged when the pH of the solution is higher than 6.3. At the same time, when the pH of the solution is 2~10, the main form of Sb(III) in the solution is the neutral complex $Sb(OH)_3$, and under strong acidic and basic conditions, their main forms are SbO^+ and SbO^{2-}, respectively (Watkins et al. 2006, Sarı et al. 2010). Therefore, when pH<3.0, the positively charged SbO^+ gradually increased with the decrease of pH, and the same positively charged γ-Fe_2O_3 magnetic microspheres could not fully contact with each other due to electrostatic repulsion, so they could not fully perform the coordination function to remove Sb(III); correspondingly, when pH>9.0, γ-Fe_2O_3 magnetic microspheres showed negative electrical properties, and the anion SbO^{2-} in the system increased correspondingly with the increase of pH, resulting in the removal efficiency of Sb(III) decreased. Considering that when pH 7.0, the removal efficiency of γ-Fe_2O_3 magnetic microspheres on Sb(III) is up to 97.8±1.5%, pH of 7.0 was selected for the subsequent experiments.

Influence of contact time

Contact time is another major factor affecting the removal of target pollutants by the adsorbent. The experimental data in this part can provide important information for the study of adsorption kinetics. When the reaction temperature is 298.15 K, the removal efficiency of Sb(III) by the nanosheet-assembled

maghemite magnetic microspheres in a contact time of 12 h is shown in Fig. 10. In this part, the absorbent with a dry weight of 200 mg was added to Sb(III) solution with an initial concentration of 10 mg/L at a pH value of 7.0, and a series of adsorption experiments were performed on a rotary shaker (150 rpm). The remaining Sb(III) concentration in the solution was measured at regular intervals.

As shown in Fig. 10, in the initial stage of adsorption with a contact time of 0-60 minutes, the removal efficiency of Sb(III) by γ-Fe_2O_3 magnetic microspheres increased rapidly, and the removal efficiency reached 81.9±0.4% when the contact time was 15 minutes; as the reaction continued, the adsorption efficiency gradually slowed down; when t=240 min, the adsorption reaction reached equilibrium, at which time the removal efficiency reached 99.9±0.3%, and almost all Sb(III) in the solution was adsorbed by γ-Fe_2O_3 magnetic microspheres. The adsorption of Sb(III) on maghemite magnetic microspheres may involve two steps. First, Sb(III) migrates from solution to the surface of the adsorbent for contact (external diffusion)(Singh et al. 1993), and second, Sb(III) is fully bind to the active sites on the surface of the adsorbent by electrostatic attraction(Chowdhury et al. 2012). The rapid adsorption of Sb(III) by the nanosheet-assembled maghemite magnetic microspheres at the beginning of the reaction is attributed to the sufficient unoccupied adsorption sites(Ahmadi et al. 2017). As the adsorption sites are gradually occupied, the repulsive force between the solid and liquid phases gradually increases(Zhang et al. 2018), and the adsorption rate of the adsorbent for Sb(III) gradually decreases and then reaches the adsorption equilibrium. In summary, t=240 min was selected as the best contact time.

Adsorption kinetics

The study on the kinetics of Sb(III) adsorption solution by nanosheet-assembled maghemite magnetic microspheres is conducive to further analysis of its adsorption mechanism.

Fig. 11 shows the kinetic fitting results of Sb(III) adsorption by γ-Fe_2O_3 magnetic microspheres. As

312 can be seen from the figure, the correlation coefficients of pseudo-first order kinetic and the pseudo-
313 second order kinetic were 0.6782 and 0.9459, respectively, and the adsorption capacities were 4.9857
314 and 5.1111, respectively. Compared with the pseudo-first order kinetic model, the pseudo-second order
315 kinetic model can more accurately describe the adsorption of Sb(III) by maghemite magnetic
316 microspheres, indicating that the adsorption process is mainly chemical adsorption, and the concentration
317 of reactants is the main factor limiting reaction.

318 ## Adsorption isotherms

319 The adsorption isotherm reflects the change of the adsorption capacity with the equilibrium
320 concentration under a certain temperature condition, which is of great significance for studying the
321 interaction between the adsorbent and the adsorbent and determining the adsorption performance of the
322 adsorbent. Langmuir model assumes that adsorption is uniform, and the effect of the adsorbent on the
323 adsorbate is monolayer surface adsorption(Saleh et al. 2017). Freundlich is an empirical equation, which
324 is mainly used to describe multiple adsorptions(Chen et al. 2015).

325 The solution was controlled to pH=7.0, and nanosheet-assembled maghemite magnetic
326 microspheres with a dry weight of 200 mg were added to 100 mL of different concentrations
327 (10~200mg/L) of Sb(III)-containing aqueous solutions at 298.15 K, 308.15 K, 318.15 K on a rotary
328 shaker (150 rpm) for 240 min, magnetic separation for 2 min after the completion of the adsorption
329 reaction, and then the supernatant was filtered through a 0.45 μm filter membrane and the remaining
330 Sb(III) concentration in the solution was detected. The data were fitted by Langmuir model (Fig. 12a)
331 and Freundlich model (Fig. 12b), and the specific parameters of the equation Q_0, K_L, K_F, R^2, 1/n are listed
332 in Table 1.

333 **Table 1** The isotherm parameters of Sb(III) adsorbed by γ-Fe_2O_3 magnetic microspheres.

T(K)	Langmuir isotherm			Freundlich isotherm		
	Q_0(mg/g)	K_L	R^2	K_F	1/n	R^2
298.18	47.48	0.0865	0.9516	9.5169	0.3416	0.9686
308.18	44.27	0.0549	0.9099	7.6426	0.3505	0.9509
318.18	35.95	0.0525	0.8806	6.4417	0.3375	0.9391

From the fitting results in Fig. 12 and the non-linear isotherm constants and correlation coefficients in Table 1, It can be seen that under the conditions of 298.18 K, 308.18 K and 318.18 K, the adsorption of Sb(III) from aqueous solution on nanosheet-assembled maghemite magnetic microspheres was obviously better described by Freundlich isotherm adsorption model (R^2 = 0.9686, 0.9509, and 0.9391) than by the Langmuir model(R^2 = 0.9516, 0.9099, and 0.8806)(Mirbagheri and Sabbaghi 2018). which indicated that the adsorption of Sb(III) on the surface of nanosheet-assembled maghemite magnetic microspheres followed the multilayer adsorption, and the adsorption process is dominated by chemical adsorption(Xiao et al. 2018). Besides, the values of R_L in Langmuir model and 1/n in Freundlich models are between 0 and 1, which indicates that the adsorption of Sb(III) onto nanosheet-assembled maghemite magnetic microspheres was favorable(Acar and Malkoc 2004, Zhang et al. 2018), the γ-Fe_2O_3 microspheres prepared in this study shows a high affinity for Sb(III).

In addition, the theoretical saturation adsorption capacity Q_0 of nanosheet-assembled γ-Fe_2O_3 magnetic microspheres for Sb(III) were 47.48, 44.27, and 35.95 mg/g at three temperature conditions. It can be concluded that the increase in temperature is not conducive to the progress of the adsorption reaction, the main reason is that the increase in temperature causes the adsorption equilibrium to move to the left. Therefore, it is speculated that the adsorption reaction is an exothermic reaction, and according to the graph, it can be seen that as the temperature gradually increases, the rate at which its adsorption performance decreases gradually increases.

The actual maximum adsorption capacity of nanosheet-assembled γ-Fe_2O_3 magnetic microspheres under optimal experimental conditions was 47.78 mg/g, which has a larger adsorption capacity than the previously reported Sb(III)-absorbing materials, as shown in Table 2. At the same time, considering the advantages of facile preparation and easy physical separation from treatment system, it has great potential for future to treat polluted waste water.

Table 2 Comparison of the sorption capacity of various sorbents toward Sb(III).

Adsorbents	Capacity (mg/g)	pH	Temperature (℃)	Equilibrium time	Ref
MNP@hematite	36.7	7.0	25	120 min	(Shan et al. 2014)
α-Fe_2O_3	23.23	4.0	20	24 h	(Guo et al. 2014)
γ-FeOOH	33.08	4.0	20	24 h	(Guo et al. 2014)
PVA-Fe^0	6.99	7.0	25	48 h	(Zhao et al. 2014)
graphene	10.919	11.0	30	240 min	(Leng et al. 2012)
iron-coated cork granulates	5.8	6.0	20	24 h	(Pintor et al. 2020)
γ-Fe_2O_3 magnetic microspheres	47.48	7.0	25	240 min	This work

Thermodynamics analysis

In order to further illustrate the spontaneous characteristics of the adsorption reaction and the energy change in the solid-liquid system. The Gibbs free energy change (ΔG^0), standard enthalpy change (ΔH^0) and entropy change (ΔS^0) were calculated. The Van't Hoff's plots and thermodynamic parameters are given in Fig. 13 and Table 3, respectively.

Table 3 Thermodynamic parameters for Sb(III) adsorbed on γ-Fe_2O_3

Temperature (K)	ΔG^0 (kJ/mol)	ΔH^0 (kJ/mol)	ΔS^0 [J/(mol·K)]
298.15	-1.715	-30.77	-0.0965
308.15	-0.746		

	318.15	-0.235

The negative values of ΔG^0 indicated that the adsorption of Sb(III) on nanosheet-assembled γ-Fe_2O_3 magnetic microspheres is a spontaneous process, and the absolute value of ΔG^0 gradually decreases with the increase of temperature, indicating that the increase of temperature is not conducive to the adsorption reaction(Ruan et al. 2020). Besides, the negative values of ΔH also indicated that the adsorption process is an exothermic reaction(Georgieva et al. 2020), which was in good agreement with the variation trend of the theoretical saturation adsorption capacity at different temperatures obtained by the Langmuir model. $\Delta S^0<0$ means that the randomness of the solid-liquid system decreases during the adsorption process. In addition, studies have shown that when the absolute value of ΔH^0 is in the range of 0 ~ 20 kJ/mol, the adsorption process is physical adsorption, and when the value is in the range of 40 ~ 80 kJ/mol, it is chemical adsorption(Zhang et al. 2019). In this study, the absolute value of ΔH^0 is 30.77 kJ/mol, indicating that the adsorption process involves multiple binding mechanisms, including both physical adsorption and chemical adsorption.

Effect of coexisting ions

There are many cations and anions in actual wastewater, which may affect the adsorption performance of adsorbents. Therefore, the effects of three competitive cations (Na^+, Ca^{2+}, Mg^{2+}) and three competitive anions (Cl^-, CO_3^{2-}, PO_4^{3-}) on Sb(III) removal by γ-Fe_2O_3 magnetic microspheres were studied at 1 mM and 10 mM concentrations. The dose of the adsorbent was controlled to 200 mg, the initial concentration of Sb(III) was 10 mg/L, the pH of the solution was 6 and the temperature was 298.15 K. The experimental results are shown in Fig. 14.

Obviously, the competitive cations of Na^+, Ca^{2+}, Mg^{2+} and the anion Cl^- have little effect on the Sb(III) removal performance of γ-Fe_2O_3 magnetic microspheres at two different concentrations, which

is similar to previous studies(Hao et al. 2019, Zhu et al. 2019). However, under the influence of two competitive anions, CO_3^{2-} and PO_4^{3-}, the removal efficiency of Sb(III) decreased slightly. When the concentration of CO_3^{2-} and PO_4^{3-} was 10 mM, the removal efficiency of Sb(III) by γ-Fe_2O_3 magnetic microspheres decreased from 99.9±2.3% to 93.7±2.2% and 90.4±1.1%, respectively. Some studies have shown that CO_3^{2-} and PO_4^{3-} could form inner-sphere complex with ferric (hydr) oxides(Shan et al. 2014, Zhang et al. 2009), which may compete with Sb(III) for adsorption sites, resulting in a decrease in the removal efficiency of Sb(III). In general, under the influence of these six coexisting ions, γ-Fe_2O_3 magnetic microspheres could still maintain high removal efficiencies (above 90%) for Sb(III) in the solution. Therefore, it can be concluded that the nanosheet-assembled γ-Fe_2O_3 magnetic microspheres have good anti-interference ability for coexisting ions in water, and it could be as a promising adsorbent to treat antimony-containing wastewaters.

Reusability test

The study on the desorption and regeneration performance of the adsorbent is an important condition for its application to the actual antimony-containing industrial wastewater. In this study, the NaOH solution was used as the eluent. The experimental process is briefly described as follows: 200 mg of nanosheet-assembled γ-Fe_2O_3 magnetic microspheres were added to 100 mL of Sb(III) solution at a concentration of 10.0 mg/L for adsorption experiments. After each reaction was completed, the adsorbent was eluted with NaOH solution (1.0M) for 20 minutes, and then washed several times with deionized water for the next regeneration experiment. Five regeneration experiments were performed in sequence. The results are shown in Fig. 15.

The figure shows that after five adsorption-desorption experiments, the removal efficiency of Sb(III) in the solution by the nanosheet-assembled γ-Fe_2O_3 magnetic microspheres decreased by about 24.4%,

but the removal efficiency of Sb(III) remains above 75.0%. It shows that the synthesized nanosheet-assembled maghemite magnetic microspheres have excellent adsorption and removal performance of Sb(III), and good desorption and regeneration effects. It is an adsorption material with practical application potential and high recyclability.

Mechanism for enhanced Sb(III) removal

According to the above results, the adsorption of Sb(III) by synthesized nanosheet-assembled γ-Fe_2O_3 magnetic microspheres is mainly chemical adsorption, accompanied by physical adsorption. In fact, the adsorption of Sb(III) is an extremely complicated process, and it is speculated that it may include multiple adsorption mechanisms such as redox, complexation, and physical adsorption. The proposed enhanced removal mechanism of Sb(III) by nanosheet-assembled γ-Fe_2O_3 magnetic microspheres is shown in Scheme 1.

Specifically, (1) combining with the high-resolution Fe 2p and Sb 3d spectrum in XPS analysis, it can be known that Fe gains electrons, and it is speculated that γ-Fe_2O_3 and Sb (III) have undergone a redox reaction, so that part of Sb(III) is oxidized to Sb(V); (2) physical adsorption, such as pore effect and electrostatic effect, although weak, may also include both in the adsorption process; (3) Sb and the lattice oxygen (O_X^{2-}) form Fe-O-Sb coordination bonds through sharing electron pairs, which is incorporated into the crystal structure of γ-Fe_2O_3 as inner-sphere surface complexes, and the chemical adsorption process may dominate the enhance removal of Sb(III) by γ-Fe_2O_3 magnetic microspheres.

Conclusion

The iron alkoxide precursor was obtained through an ethylene glycol (EG)- mediated self-assembly process, and then it was calcined in air at high temperature to successfully synthesize γ-Fe_2O_3 magnetic microspheres with high specific surface area. This method is fast, simple, and low cost. Batch adsorption

experiments found that nanosheet-assembled γ-Fe_2O_3 magnetic microspheres have excellent adsorption effect on Sb(III), and have a wide range of adaptation to pH value. In the range of pH 1~11, the removal efficiencies are all above 90.3±0.8%. When pH=7 and temperature is 298.15 K, the maximum adsorption capacity of the material is 47.48 mg/g. After the adsorption reaction is completed, the adsorption material can quickly achieve solid-liquid separation under the action of an external magnetic field, which greatly reduces the operating cost of practical applications. After five adsorption-desorption experiments, the adsorbent still has effective removal of Sb(III) demonstrating that the nanosheet-assembled γ-Fe_2O_3 magnetic microspheres is an excellent material for antimony removal.

Ethical approval and consent to participate Not applicable.

Consent for publication Not applicable.

Competing interests The authors declare that they have no competing interests.

Authors Contributions B R and W Z contributed to the study design. Measurement preparation, experiments, data collection and analysis were performed by W Z. The first draft of the manuscript was written by W Z. A H checked the quality of the English and critically revised the work. A H and Z W commented on previous versions of the manuscript and provided valuable reviews. All authors read and approved the final manuscript.

Funding information This work was supported by the National Natural Science Foundation of China (Nos. 41973078) and the Ministry of Education in China Project of Humanities and Social Science (2019JJ40081).

Data availability All data generated or analyzed during this study are included in this published article.

References

Abdullah NH, Shameli K, Abdullah EC, Abdullah LC (2019) Solid matrices for fabrication of magnetic iron oxide nanocomposites: Synthesis, properties, and application for the adsorption of heavy metal ions and dyes. Compos Pt B-Eng 162:538-568. https://doi.org/10.1016/j.compositesb.2018.12.075

Acar FN, Malkoc E (2004) The removal of chromium(VI) from aqueous solutions by Fagus orientalis L. Bioresour Technol 94(1) :13-15. https://doi.org/10.1016/j.biortech.2003.10.032

Ahmadi M, Hazrati Niari M, Kakavandi B (2017) Development of maghemite nanoparticles supported on cross-linked chitosan (γ-Fe_2O_3@CS) as a recoverable mesoporous magnetic composite for effective heavy metals removal. J Mol Liq 248:184-196. https://doi.org/10.1016/j.molliq.2017.10.014

Bulin C, Li B, Zhang Y, Zhang B (2020) Removal performance and mechanism of nano α-Fe_2O_3/graphene oxide on aqueous Cr(VI). J Phys Chem Solids 147:109659. https://doi.org/10.1016/j.jpcs.2020.109659

Chen H, Li T, Zhang L, Wang R, Jiang F, Chen J (2015) Pb(II) adsorption on magnetic γ-Fe2O3/titanate nanotubes composite. J Environ Chem Eng 3(3):2022-2030. https://doi.org/10.1016/j.jece.2015.07.010

Chowdhury SR, Yanful EK, Pratt AR (2012) Chemical states in XPS and Raman analysis during removal of Cr(VI) from contaminated water by mixed maghemite–magnetite nanoparticles. J Hazard Mater 235-236:246-256. https://doi.org/10.1016/j.jhazmat.2012.07.054

Fiore M, Longoni G, Santangelo S, Pantò F, Stelitano S, Frontera P, Antonucci P, Ruffo R (2018) Electrochemical characterization of highly abundant, low cost iron (III) oxide as anode material for sodium-ion rechargeable batteries. Electrochim Acta 269:367-377. https://doi.org/10.1016/j.electacta.2018.02.161

Flak D, Chen Q, Mun BS, Liu Z, Rękas M, Braun A (2018) In situ ambient pressure XPS observation of surface chemistry and electronic structure of α-Fe_2O_3 and γ-Fe_2O_3 nanoparticles. Appl Surf Sci 455:1019-1028. https://doi.org/10.1016/j.apsusc.2018.06.002

Ge J, Hu Y, Biasini M, Beyermann W, Yin Y (2007) Superparamagnetic Magnetite Colloidal Nanocrystal Clusters. Angew Chem Int Edit 119(23):4420-4423. https://doi.org/10.1002/ange.200700197

Georgieva VG, Gonsalvesh L, Tavlieva MP (2020) Thermodynamics and kinetics of the removal of nickel (II) ions from aqueous solutions by biochar adsorbent made from agro-waste walnut shells. J Mol Liq 312:112788. https://doi.org/10.1016/j.molliq.2020.112788

Guo W, Fu Z, Wang H, Liu Sha, Wu Feng, Giesy JP (2018) Removal of antimonate (Sb(V)) and antimonite (Sb(III)) from aqueous solutions by coagulation-flocculation-sedimentation (CFS): Dependence on influencing factors and insights into removal mechanisms. Sci Total Environ 644:1277-1285. https://doi.org/10.1016/j.scitotenv.2018.07.034

Guo X, Wu Z, He M, Meng X, Jin X, Qiu N, Zhang J (2014) Adsorption of antimony onto iron oxyhydroxides: Adsorption behavior and surface structure. J Hazard Mater 276(15):339-345. https://doi.org/10.1016/j.jhazmat.2014.05.025

Gusain R, Kumar N, Ray SS (2020) Recent advances in carbon nanomaterial-based adsorbents for water purification. Coord Chem Rev 405:213111. https://doi.org/10.1016/j.ccr.2019.213111

Hao H, Liu G, Wang Y, Shi B, Han K, Zhuang Y, Kong Y (2019) Simultaneous cationic Cu(II)−anionic

Sb(III) removal by NH_2-Fe_3O_4-NTA core-shell magnetic nanoparticle sorbents synthesized via a facile one-pot approach. J Hazard Mater 362:246-257. https://doi.org/10.1016/j.jhazmat.2018.08.096

Hao Y, Man C, Hu Z (2010) Effective removal of Cu (II) ions from aqueous solution by amino-functionalized magnetic nanoparticles. J Hazard Mater 184(1-3):392-399. https://doi.org/10.1016/j.jhazmat.2010.08.048

He M, Wang N, Long X, Zhang C, Ma C, Zhong Q, Wang A, Wang Y, Pervaiz A, Shan J (2019) Antimony speciation in the environment: Recent advances in understanding the biogeochemical processes and ecological effects. J Environ Sci 75:14-39. https://doi.org/10.1016/j.jes.2018.05.023

Jordan N, Ritter A, Scheinost A, Weiss S, Dieter S, René H (2014) Selenium(IV) uptake by maghemite (γ-Fe_2O_3). Environ Sci Technol 48(3):1665-1674. https://doi.org/10.1021/es4045852

Khosravi M, Azizian S (2014) Synthesis of different nanostructured flower-like iron oxides and study of their performance as adsorbent. Adv Powder Technol 25(5):1578-1584. https://doi.org/10.1016/j.apt.2014.05.010

Kirsch R, Scheinost AC, Rossberg A, Banerjee D, Charlet L (2008) Reduction of antimony by nano-particulate magnetite and mackinawite. Mineral Mag 72:185-189. https://doi.org/10.1180/minmag.2008.072.1.185

Leng Y, Guo W, Su S, Yi C, Xing L (2012) Removal of antimony(III) from aqueous solution by graphene as an adsorbent. Chem Eng J 211-212:406-411. https://doi.org/10.1016/j.cej.2012.09.078

Li J, Zheng B, He Y, Zhou Y, Chen X, Ruan S, Yang Y, Dai C, Tang L (2018a) Antimony contamination, consequences and removal techniques: A review. Ecotox Environ Safe. 156:125-134. https://doi.org/10.1016/j.ecoenv.2018.03.024

Li J, Guo R, Ma Q, Nengzi L, Cheng X et al (2019) Efficient removal of organic contaminant via activation of potassium persulfate by γ-Fe_2O_3/α-MnO_2 nanocomposite. Sep Purif Technol 227:115669. https://doi.org/10.1016/j.seppur.2019.06.007

Li M, Liu H, Zhu H, Gao H, Zhang S, Chen T (2017) Kinetics and mechanism of Sr(II) adsorption by Al-Fe_2O_3: Evidence from XPS analysis. J Mol Liq 233:364-369. https://doi.org/10.1016/j.molliq.2017.03.045

Li W, Fu F, Ding Z, Tang B (2018b) Zero valent iron as an electron transfer agent in a reaction system based on zero valent iron/magnetite nanocomposites for adsorption and oxidation of Sb(III). J Taiwan Inst Chem Eng 85:155-164. https://doi.org/10.1016/j.jtice.2018.01.032

Liu W, Ma J, Chen K (2015) Micron-size superparamagnetic iron-oxides watercress with unique MRI properties. Mater Chem Phys 170:123-128. https://doi.org/10.1016/j.matchemphys.2015.12.029

Ma J, Zhou G, Chu L, Liu Y, Liu C, Luo S, Wei Y (2016) Efficient removal of heavy metal ions with EDTA functionalized chitosan/polyacrylamide double network hydrogel. ACS Sustain Chem Eng 5(1):843-851. https://doi.org/10.1021/acssuschemeng.6b02181

Ma X, Feng X, Song C, Zou B, Ding C, Yu Y, Chen C (2013) Facile synthesis of flower-like and yarn-like α-Fe_2O_3 spherical clusters as anode materials for lithium-ion batteries. Electrochim Acta 93:131-136. https://doi.org/10.1016/j.electacta.2013.01.096

Ma Z, Shan C, Liang J, Tong M (2018) Efficient adsorption of Selenium(IV) from water by hematite modified magnetic nanoparticles. Chemosphere 193:134-141. https://doi.org/10.1016/j.chemosphere.2017.11.005

Mirbagheri NS, Sabbaghi S (2018) A natural kaolin/γ-Fe_2O_3 composite as an efficient nano-adsorbent for removal of phenol from aqueous solutions. Microporous Mesoporous Mat 259:134-141.

https://doi.org/10.1016/j.micromeso.2017.10.007
Morin G, Ona-Nguema G, Wang Y, Menguy N, Brown GE (2008) Extended X-ray Absorption Fine Structure Analysis of Arsenite and Arsenate Adsorption on Maghemite. Environ Sci Technol 42(7):2361-2366. https://doi.org/10.1021/es072057s
Nishiyama SY, Saito K, Saito K et al (2003) High-speed recovery of antimony using chelating porous hollow-fiber membrane. J Membr Sci 214(2): 275-281. https://doi.org/10.1016/S0376-7388(02)00558-6
Niu J, Zhang Z, Dai P, Yao B, Yu X, Zhang Q, Yang R (2018) Facile synthesis of γ-Fe2O3/BiOI microflowers with enhanced visible light photocatalytic activity. Mater Des 150:29-39. https://doi.org/10.1016/j.matdes.2018.04.001
Patra D, Gopalan B, Ganesan R (2019) Direct solid-state synthesis of maghemite as a magnetically recoverable adsorbent for the abatement of methylene blue. Journal of Environmental Chemical Engineering 7(5):103384. https://doi.org/10.1016/j.jece.2019.103384
Penki TR, Shivakumara S, Minakshi M, Munichandraiah N (2015) Porous Flower-like α-Fe_2O_3 Nanostructure: A High Performance Anode Material for Lithium-ion Batteries. Electrochim Acta 167, 330-339. https://doi.org/10.1016/j.electacta.2015.03.146
Pintor AMA, Vieira BRC, Boaventura RAR, Botelho CMS (2020) Removal of antimony from water by iron-coated cork granulates. Sep Purif Technol 233:116020. https://doi.org/10.1016/j.seppur.2019.116020
Piraman S, Sundar S, Mariappan R, Kim YY, Min K (2016) Nanospheres and nanoleaves of γ-Fe_2O_3 architecturing for magnetic and biomolecule sensing applications. Sens Actuator B-Chem. 234:386-394. https://doi.org/10.1016/j.snb.2016.04.168
Qi Z, Lan H, Prasai Joshi T, Liu R, Liu H, Qu J (2016) Enhanced Oxidative and Adsorptive Capability towards Antimony by Copper-doping into Magnetite Magnetic particles. RSC Adv 6:66990-67001. https://doi.org/10.1039/C6RA13412B
Qi Z, Joshi TP, Liu R, Liu H, Qu J (2017) Synthesis of Ce(III)-doped Fe_3O_4 magnetic particles for efficient removal of antimony from aqueous solution. J Hazard Mater 329:193-204. https://doi.org/10.1016/j.jhazmat.2017.01.007
Ramirez-Muñiz K, Jia F, Song S (2012) Adsorption of As(V) in aqueous solutions on porous hematite prepared by thermal modification of a siderite-goethite concentrate. Environ Chem 9(6):512-520 https://doi.org/10.1071/EN12120
Ren B, Chen Y, Zhu G, Wang Z, Zheng X (2016) Spatial Variability and Distribution of the Metals in Surface Runoff in a Nonferrous Metal Mine. J Anal Methods Chem 7:1-11. https://doi.org/10.1155/2016/4515673
Ren B, Zhou Y, Ma H, Deng R, Zhang P, Hou B (2018) Sb release characteristics of the solid waste produced in antimony mining smelting process. J MATER CYCLES WASTE Manag 20:193-200. 10.1007/s10163-016-0562-4
Ren M, Ding S, Fu Z, Yang L, Tang W, Tsang DCW, Wang D, Wang Y (2019) Seasonal antimony pollution caused by high mobility of antimony in sediments: In situ evidence and mechanical interpretation. J Hazard Mater 367:427-436. https://doi.org/10.1016/j.jhazmat.2018.12.101
Ruan B, Wu P, Liu J, Jiang L, Wang H, Qiao J, Zhu N, Dang Z, Luo H, Yi X (2020) Adhesion of Sphingomonas sp. GY2B onto montmorillonite: A combination study by thermodynamics and the extended DLVO theory. Colloid Surf B-Biointerfaces 192:111085. https://doi.org/10.1016/j.colsurfb.2020.111085

Saleh TA, Sarı A, Tuzen M (2017) Effective adsorption of antimony(III) from aqueous solutions by polyamide-graphene composite as a novel adsorbent. Chem Eng J 307:230-238. https://doi.org/10.1016/j.cej.2016.08.070

Sarı A, Çıtak D, Tuzen M (2010) Equilibrium, thermodynamic and kinetic studies on adsorption of Sb(III) from aqueous solution using low-cost natural diatomite. Chem Eng J 162(2):521-527. https://doi.org/10.1016/j.cej.2010.05.054

Shan C, Ma Z, Tong M (2014) Efficient removal of trace antimony(III) through adsorption by hematite modified magnetic nanoparticles. J Hazard Mater 268:229-236. https://doi.org/10.1016/j.jhazmat.2014.01.020

Singh DB, Gupta GS, Prasad G, Rupainwar DC (1993) The Use of Hematite for Chromium(VI) Removal. J Environ Sci Heal A 28:1813-1826. https://doi.org/10.1080/10934529309375979

Sun T, Zhu Y, Qi C, Ding G, Chen F, Wu J (2016) α-Fe_2O_3 nanosheet-assembled hierarchical hollow mesoporous microspheres: Microwave-assisted solvothermal synthesis and application in photocatalysis. J Colloid Interface Sci 463:107-117. https://doi.org/10.1016/j.jcis.2015.10.038

Tadic M, Trpkov D, Kopanja L, Vojnovic S, Panjan M (2019) Hydrothermal synthesis of hematite (α-Fe_2O_3) nanoparticle forms: Synthesis conditions, structure, particle shape analysis, cytotoxicity and magnetic properties. J Alloy Compd 792:599-609. https://doi.org/10.1016/j.jallcom.2019.03.414

Telford K, Maher W, Krikowa F, Foster S, Ellwood M, Ashley P, Lockwood P, Wilson S (2009): Bioaccumulation of antimony and arsenic in a highly contaminated stream adjacent to the Hillgrove Mine, NSW, Australia. Environ Chem 6(2):133-143. https://doi.org/10.1071/EN08097

Thommes M, Kaneko K, Neimark A, Olivier J, Rodriguez-Reinoso F, Rouquerol J, Sing K (2015): Physisorption of gases, with special reference to the evaluation of surface area and pore size distribution (IUPAC Technical Report). Pure Appl Chem 87 (9-10). https://doi.org/10.1515/pac-2014-1117

Torkashvand N, Sarlak N (2019) Synthesis of completely dispersed water soluble functionalized graphene/γ-Fe2O3 nanocomposite and its application as an MRI contrast agent. J Mol Liq 291:111286. https://doi.org/10.1016/j.molliq.2019.111286

Üçer A, Uyanik A, Aygün Ş.F (2006) Adsorption of Cu(II), Cd(II), Zn(II), Mn(II) and Fe(III) ions by tannic acid immobilised activated carbon. Sep Purif Technol 47(3):113-118. https://doi.org/10.1016/j.seppur.2005.06.012

Ungureanu G, Santos S, Boaventura R, Botelho C (2015) Arsenic and antimony in water and wastewater: Overview of removal techniques with special reference to latest advances in adsorption. J Environ Manage 151:326-342. https://doi.org/10.1016/j.jenvman.2014.12.051

Wang P, Lo IMC (2009) Synthesis of mesoporous magnetic γ-Fe_2O_3 and its application to Cr(VI) removal from contaminated water. Water Res 43(15):3727-3734. https://doi.org/10.1016/j.watres.2009.05.041

Wang T, Zhang L, Li C, Yang W, Song T, Tang C, Meng Y, Shuo D, Wang H, Chai L, Luo J (2015) Synthesis of Core–Shell Magnetic Fe_3O_4@poly(m-Phenylenediamine) Particles for Chromium Reduction and Adsorption. Environ Sci Technol 49(9):5654-5662. https://doi.org/10.1021/es5061275

Watkins R, Weiss D, Dubbin W, Peel K, Coles B, Arnold T (2006): Investigations into the kinetics and thermodynamics of Sb(III) adsorption on goethite (α-FeOOH). J Colloid Interface Sci 303(2): 639-646. https://doi.org/10.1016/j.jcis.2006.08.044

Xiao X, Yang L, Zhou D, Zhou J, Tian Y, Song C, Liu C (2018) Magnetic γ-Fe_2O_3/Fe-doped

hydroxyapatite nanostructures as high-efficiency cadmium adsorbents. Colloid Surf A-Physicochem. Eng Asp 555:548-557. https://doi.org/10.1016/j.colsurfa.2018.07.036

Xie W, Han Y, Tai S (2017) Biodiesel production using biguanide-functionalized hydroxyapatite-encapsulated-γ-Fe2O3 nanoparticles. Fuel 210:83-90. https://doi.org/10.1016/j.fuel.2017.08.054

Yamashita T, Hayes P (2008) Analysis of XPS spectra of Fe^{2+} and Fe^{3+} ions in oxide materials. Appl Surf Sci 254(8): 2441-2449. https://doi.org/10.1016/j.apsusc.2007.09.063

Zhang G, Liu H, Liu R, Qu J (2009) Removal of phosphate from water by a Fe–Mn binary oxide adsorbent. J Colloid Interface Sci 335(2):168-174. https://doi.org/10.1016/j.jcis.2009.03.019

Zhang G, Ouyang X, Li H, Fu Z, Chen J (2016) Bioremoval of antimony from contaminated waters by a mixed batch culture of sulfate-reducing bacteria. Int Biodeterior Biodegrad 115:148-155. https://doi.org/10.1016/j.ibiod.2016.08.007

Zhang H, Khanal SK, Jia Y, Song S, Lu H (2019) Fundamental insights into ciprofloxacin adsorption by sulfate-reducing bacteria sludge: Mechanisms and thermodynamics. Chem Eng J 378:122103. https://doi.org/10.1016/j.cej.2019.122103

Zhang W, Deng Q, He Q, Song J, Zhang S, Wang H, Zhou J, Zhang H (2018) A facile synthesis of core-shell/bead-like poly (vinyl alcohol)/alginate@PAM with good adsorption capacity, high adaptability and stability towards Cu(II) removal. Chem Eng J 351:462-472. https://doi.org/10.1016/j.cej.2018.06.129

Zhao X, Dou X, Mohan D, Pittman CU, Ok YS, Jin X (2014) Antimonate and antimonite adsorption by a polyvinyl alcohol-stabilized granular adsorbent containing nanoscale zero-valent iron. Chem Eng J 247:250-257. https://doi.org/10.1016/j.cej.2014.02.096

Zhong L, Hu J, Liang H, Cao A, Song W, Wan L (2006) Self-Assembled 3D Flowerlike Iron Oxide Nanostructures and Their Application in Water Treatment. Adv Mater 18(18):2426-2431 https://doi.org/10.1002/adma.200600504

Zhou Y, Ren B, Hursthouse A, Zhou S (2018) Antimony Ore Tailings: Heavy Metals, Chemical Speciation, and Leaching Characteristics. Pol J Environ Stud 28(1):485–495. https://doi.org/10.15244/pjoes/85006

Zhu K, Chen C, Wang H, Xie Y, Wakeel M, Wahid A, Zhang X (2019) Gamma-ferric oxide nanoparticles decoration onto porous layered double oxide belts for efficient removal of uranyl. J Colloid Interface Sci 535, 265-275. https://doi.org/10.1016/j.jcis.2018.10.005

Table 1 The isotherm parameters of Sb(III) adsorbed by γ-Fe_2O_3 magnetic microspheres

T(K)	Langmuir isotherm			Freundlich isotherm		
	Q_0(mg/g)	K_L	R^2	K_F	1/n	R^2
298.18	47.48	0.0865	0.9516	9.5169	0.3416	0.9686
308.18	44.27	0.0549	0.9099	7.6426	0.3505	0.9509
318.18	35.95	0.0525	0.8806	6.4417	0.3375	0.9391

Table 2 Comparison of the sorption capacity of various sorbents toward Sb(III)

Adsorbents	Capacity (mg/g)	pH	Temperature (°C)	Equilibrium time	Ref
MNP@hematite	36.7	7.0	25	120 min	(Shan et al. 2014)
α-Fe_2O_3	23.23	4.0	20	24 h	(Guo et al. 2014)
γ-FeOOH	33.08	4.0	20	24 h	(Guo et al. 2014)
PVA-Fe^0	6.99	7.0	25	48 h	(Zhao et al. 2014)
graphene	10.919	11.0	30	240 min	(Leng et al. 2012)
iron-coated cork granulates	5.8	6.0	20	24 h	(Pintor et al. 2020)
γ-Fe_2O_3 magnetic microspheres	47.48	7.0	25	240 min	This work

Table 3 Thermodynamic parameters for Sb(III) adsorbed on γ-Fe_2O_3

Temperature (K)	ΔG^0 (kJ/mol)	ΔH^0 (kJ/mol)	ΔS^0 [J/(mol·K)]
298.15	-1.715		
308.15	-0.746	-30.77	-0.0965
318.15	-0.235		

666
667

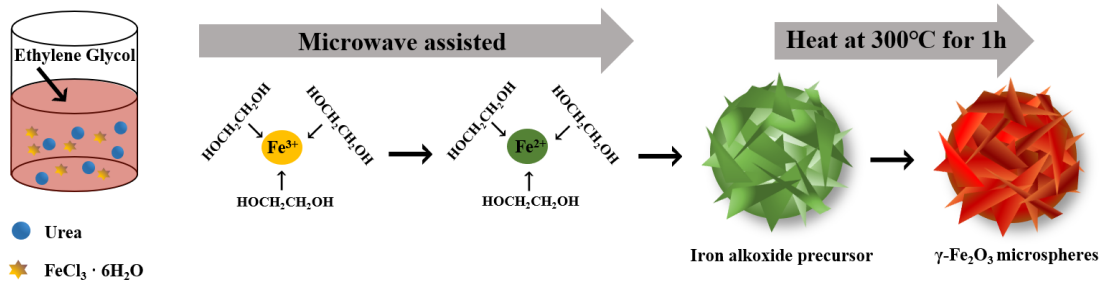

Fig. 1 The schematic diagram of synthesis process

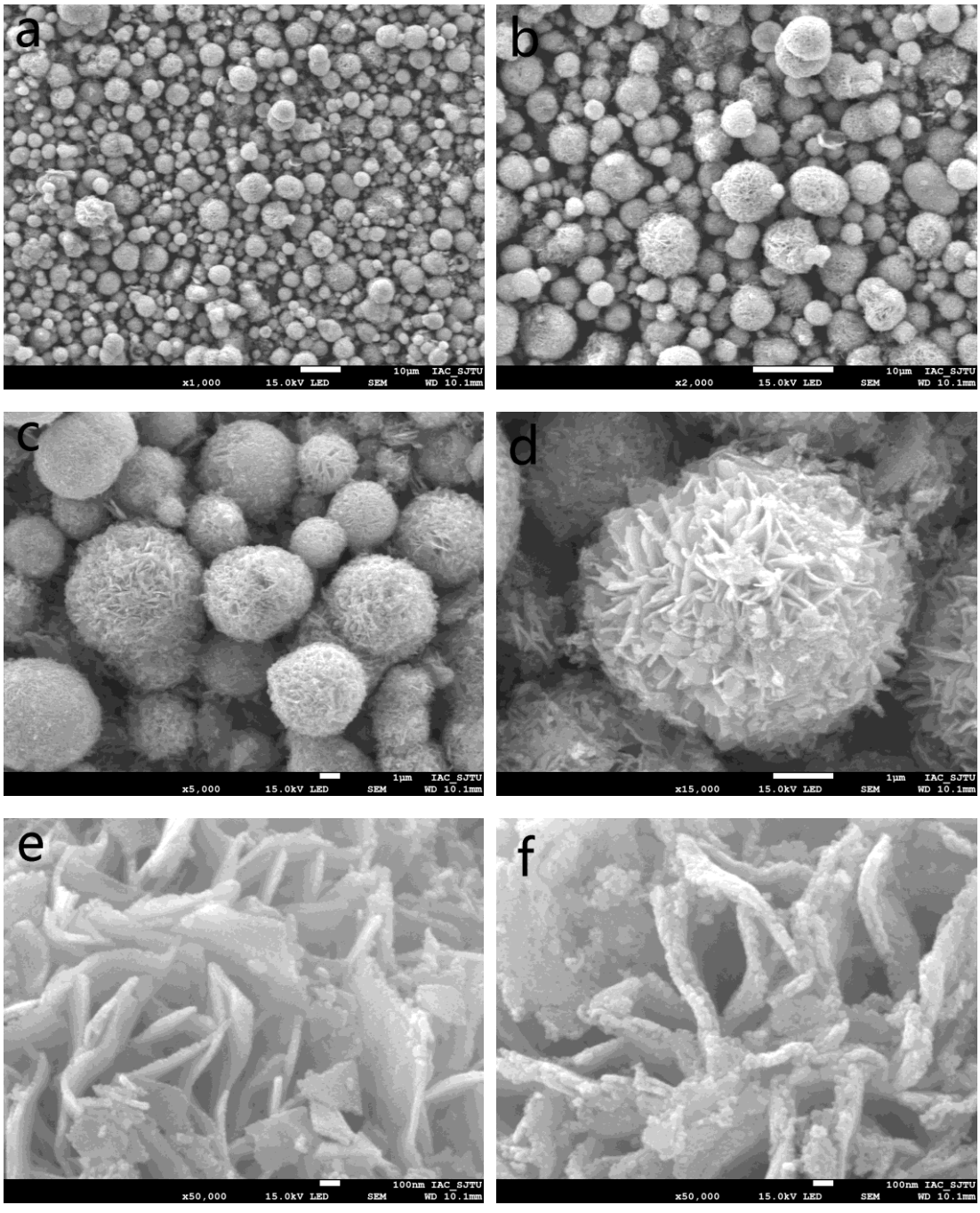

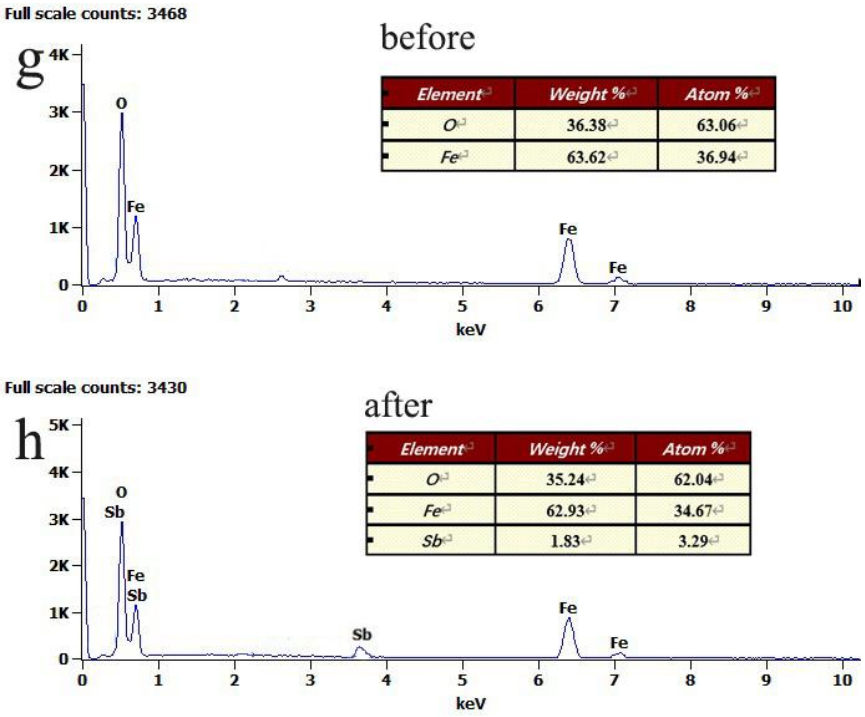

Fig. 2 SEM mapping micrographs of the product (a~e), after the product adsorbed Sb(III) (f), and EDS results of product before and after adsorption (g, h)

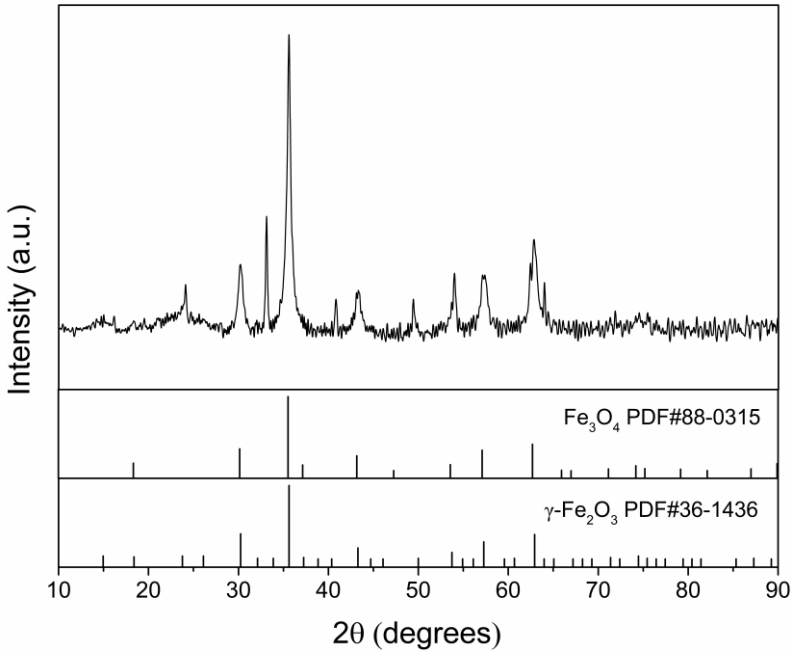

Fig. 3 XRD patterns of the product

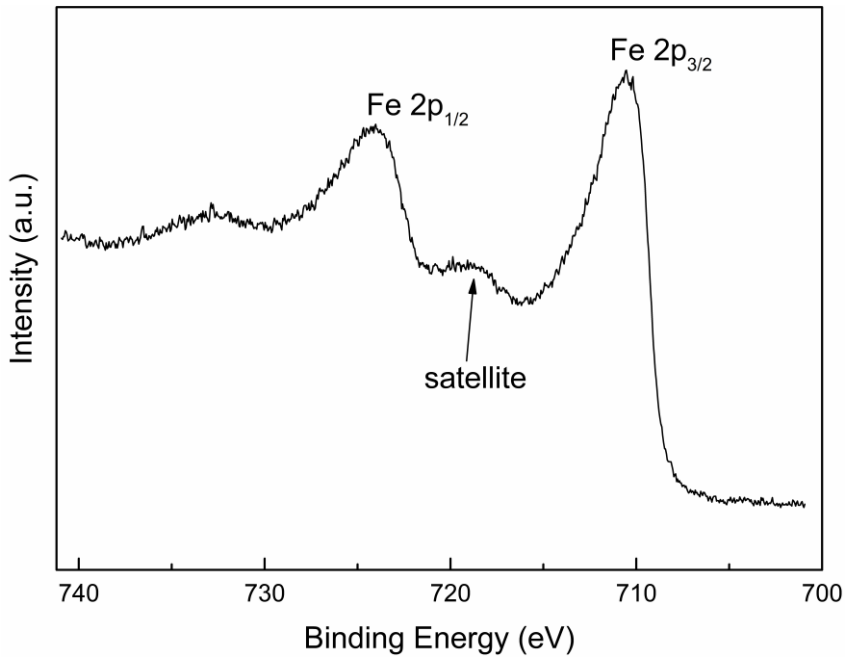

Fig. 4 XPS Fe2p of the product

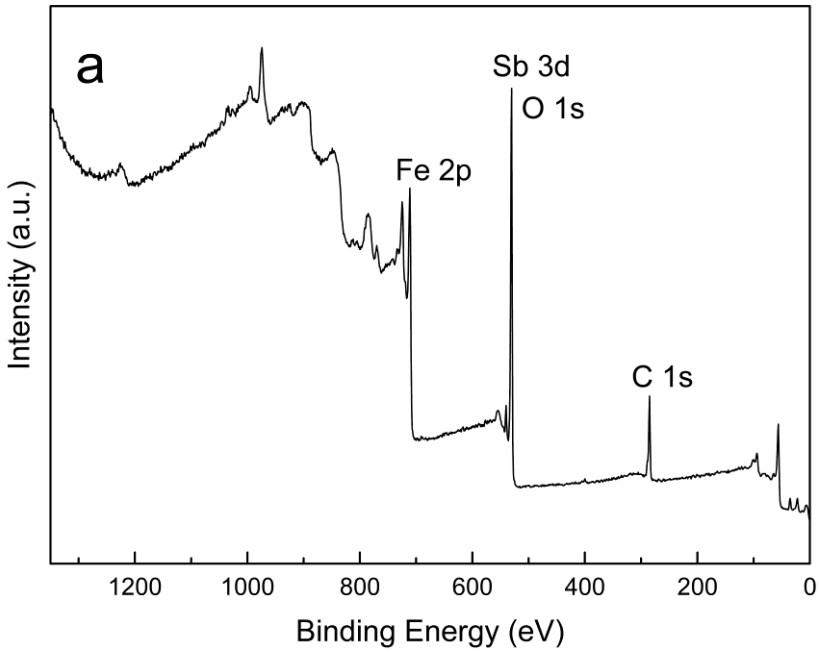

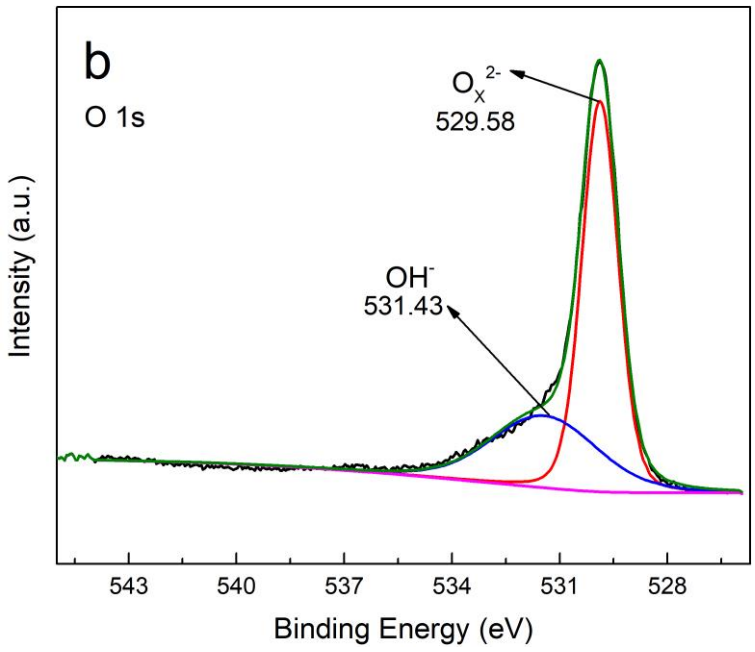
b
O 1s
O_X^{2-}
529.58
OH^-
531.43
Intensity (a.u.)
543
540
537
534
531
528
Binding Energy (eV)

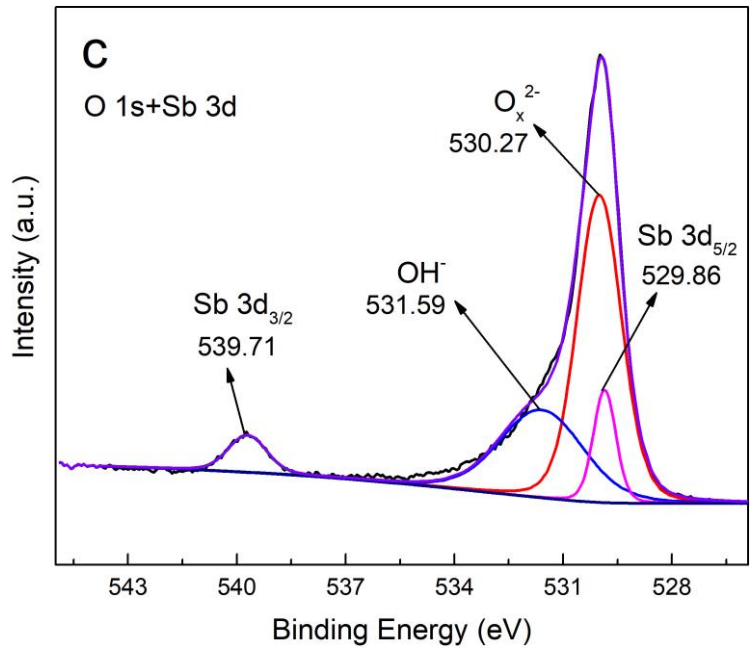
c
O 1s+Sb 3d
O_x^{2-}
530.27
$Sb\ 3d_{5/2}$
529.86
OH^-
531.59
$Sb\ 3d_{3/2}$
539.71
Intensity (a.u.)
543
540
537
534
531
528
Binding Energy (eV)

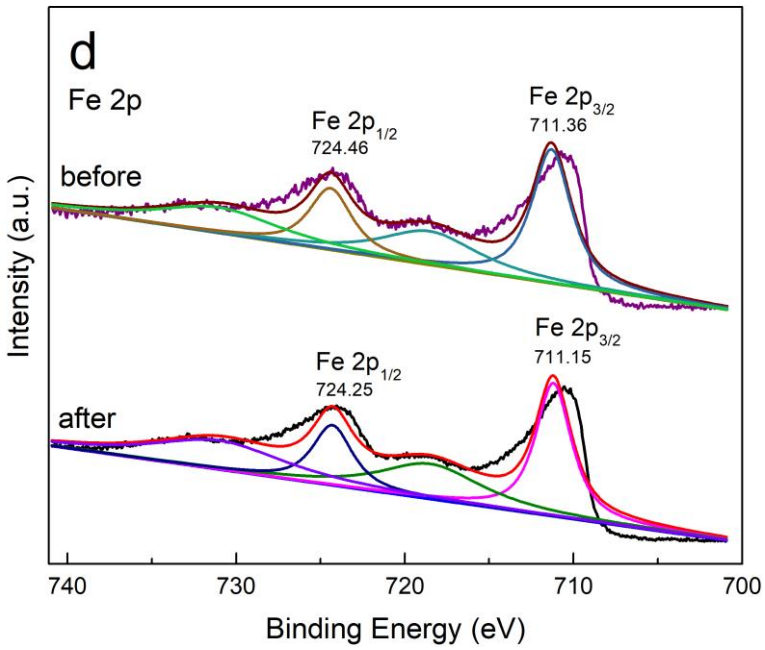

Fig. 5 (a)XPS survey spectra of full scan of γ-Fe_2O_3 after Sb(III) adsorption, (b)high-resolution O 1s before adsorption, (c) high-resolution O 1s+Sb 3d after adsorption, (c) high-resolution Fe 2p before and after adsorption

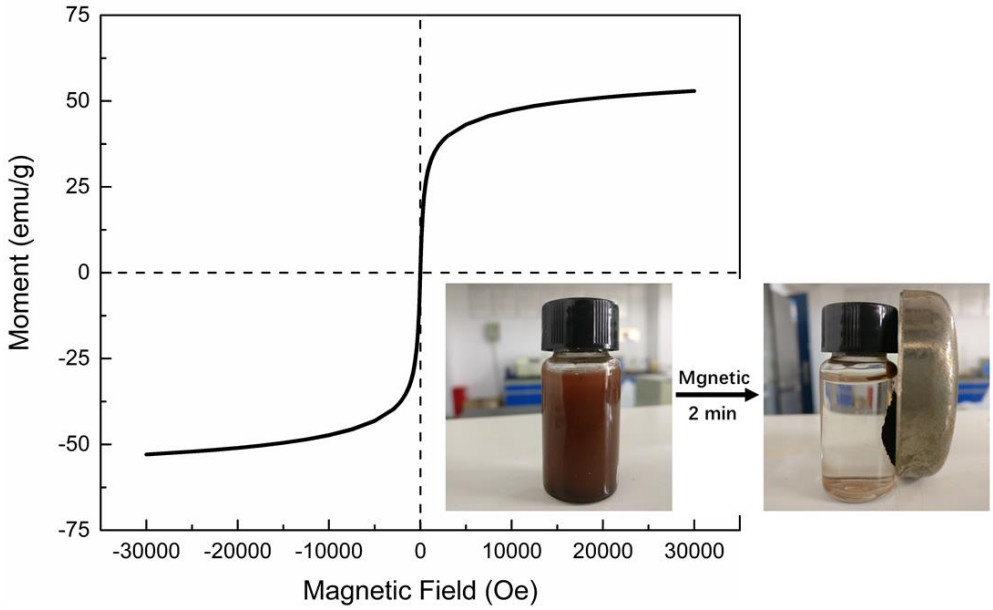

Fig. 6 Magnetic hysteresis loops of synthesized γ-Fe_2O_3 microspheres (inset pictures were the images of the microspheres dispersed in the solution and after magnet applied)

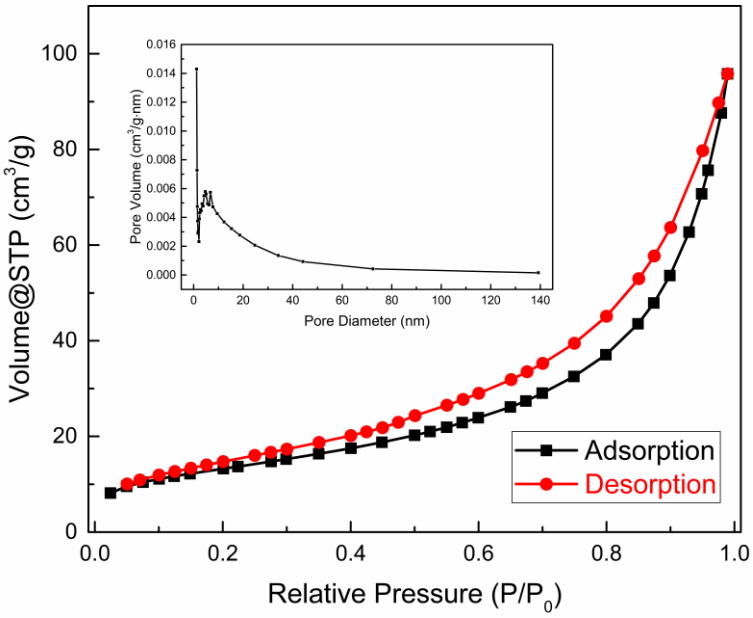

Fig. 7 Nitrogen adsorption/desorption isotherm and the BJH pore diameter distribution (inset) of the synthesized γ-Fe_2O_3 microspheres

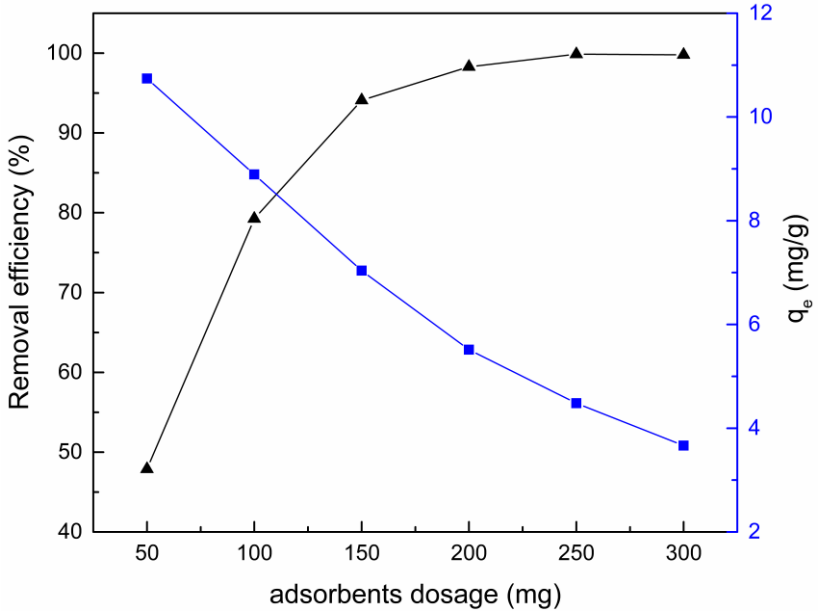

Fig. 8 The effect of dose on the Sb(III) adsorption onto γ-Fe_2O_3 magnetic microspheres

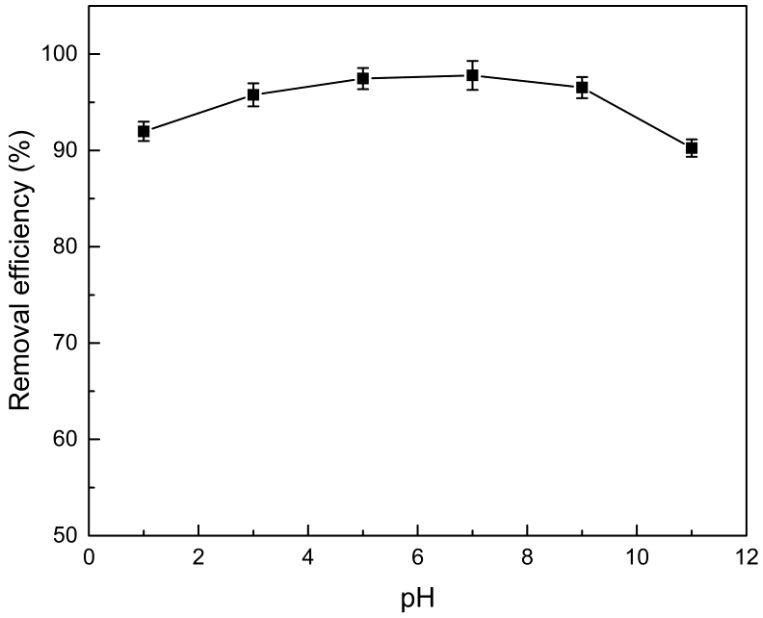

Fig. 9 The effect of pH on the Sb(III) adsorption by γ-Fe_2O_3 magnetic microspheres

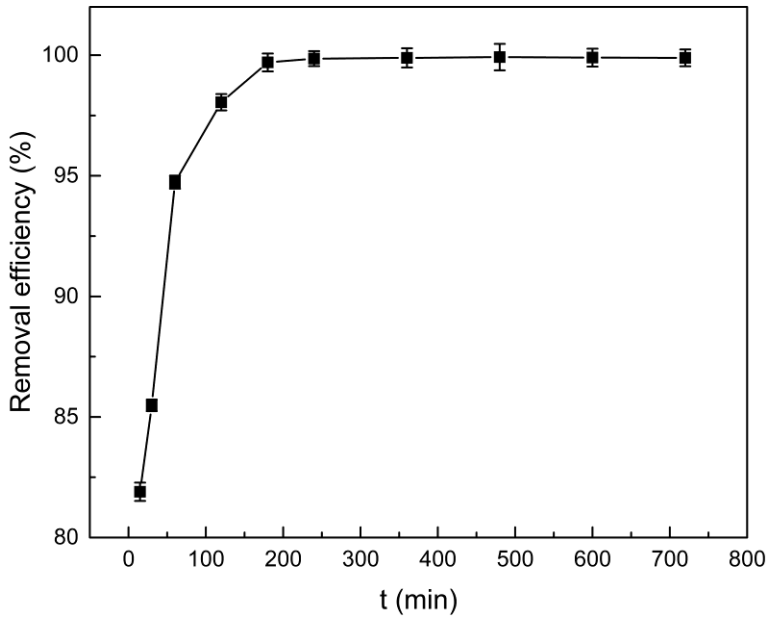

Fig. 10 The effect of contact time on the Sb(III) adsorption by γ-Fe_2O_3 magnetic microspheres

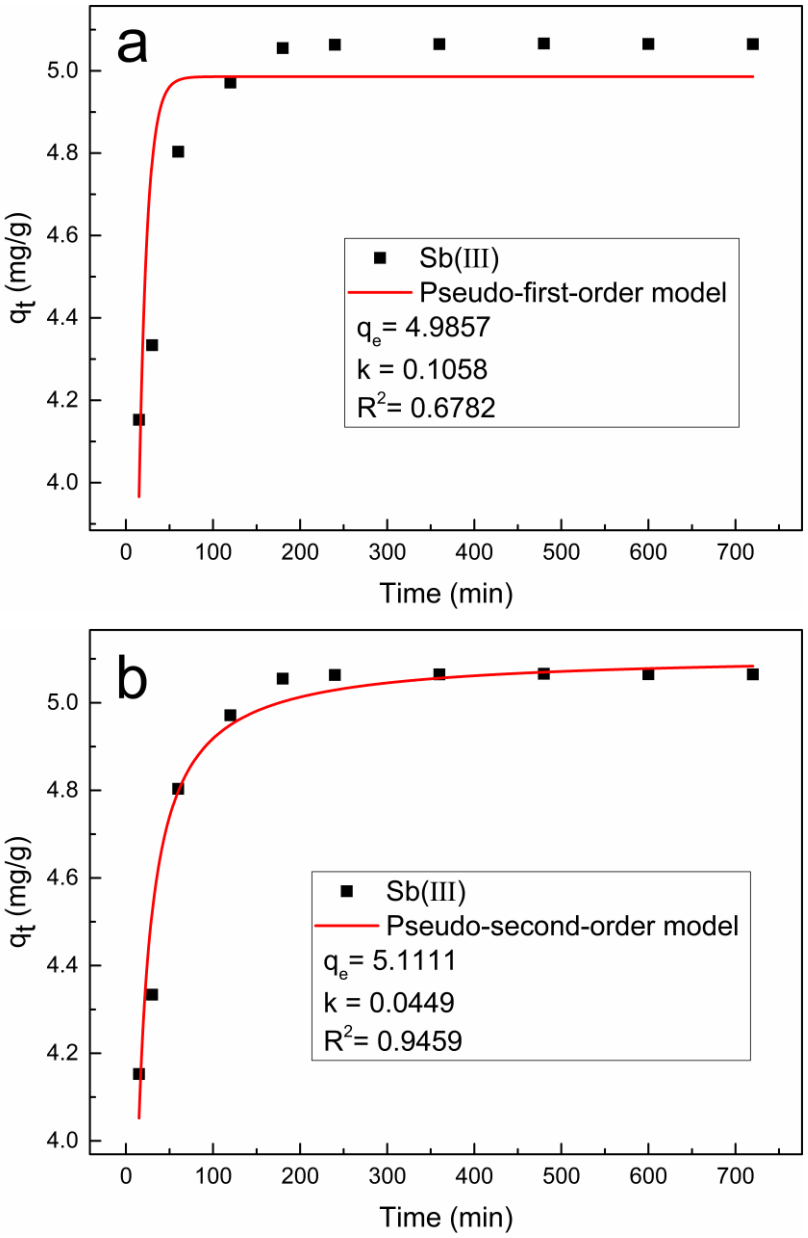

Fig. 11 The pseudo-first order kinetic (a) and pseudo-second order kinetic (b) model and parameters for Sb(III) by γ-Fe_2O_3 magnetic microspheres

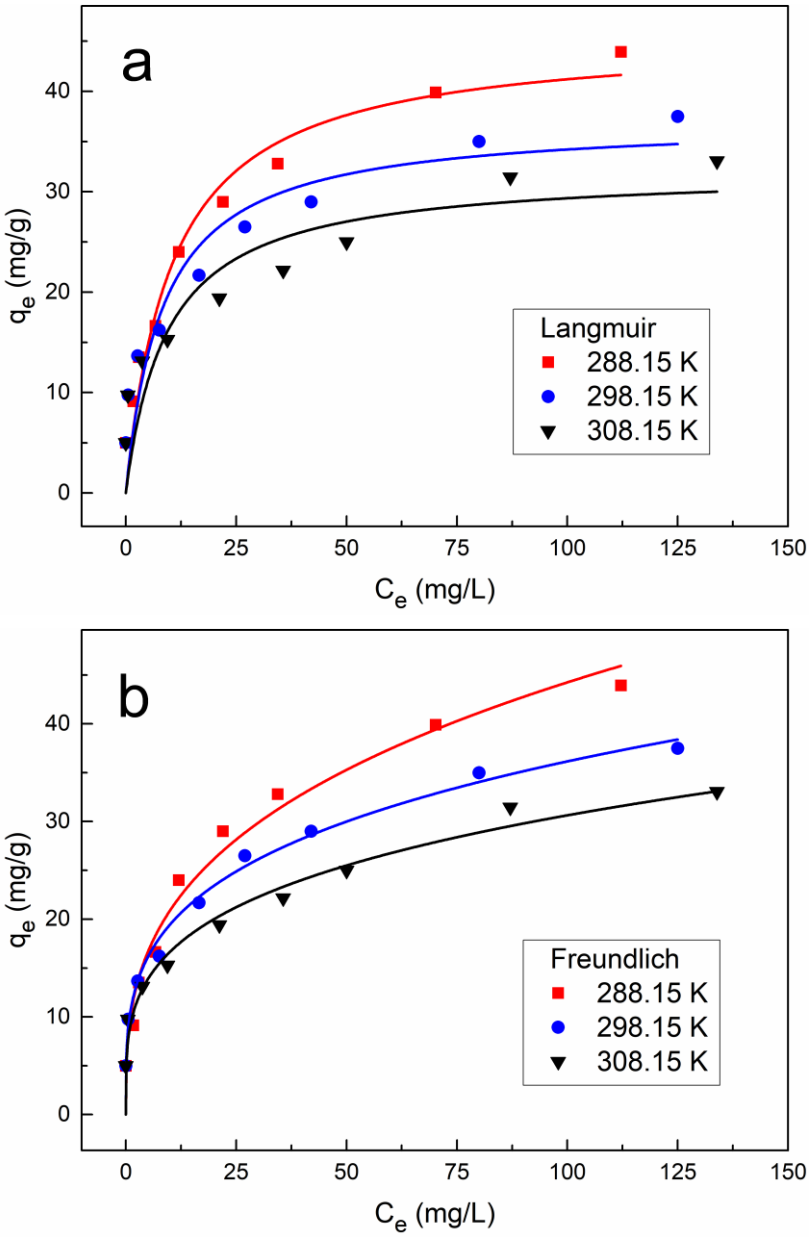

Fig. 12 Langmuir(a) and Freundlich(b) isotherms of for Sb(III) by γ-Fe_2O_3 magnetic microspheres

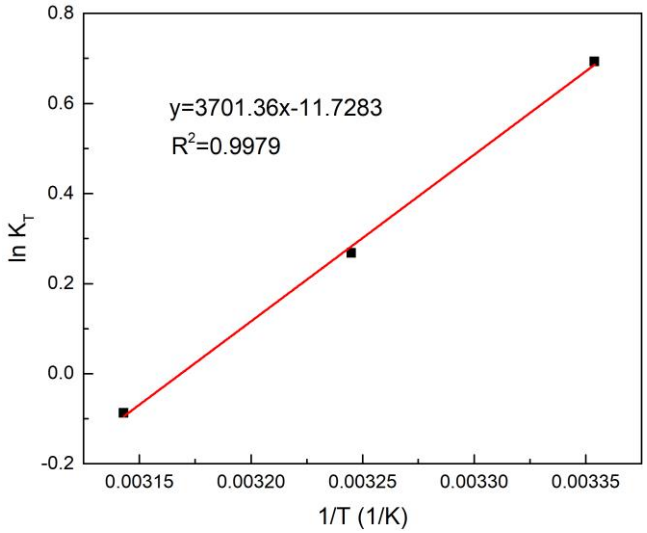

Fig. 13 The Van't Hoff plots for the adsorption of Sb(III) on γ-Fe_2O_3 magnetic microspheres

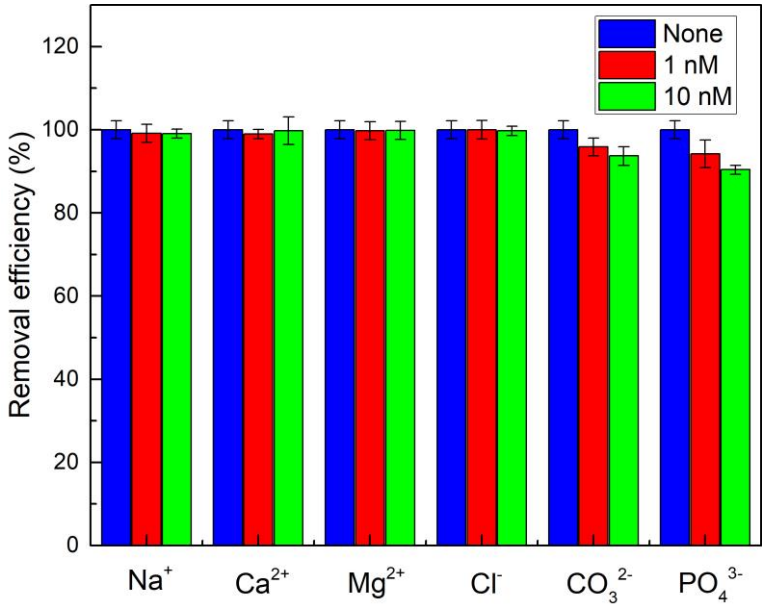

Fig. 14 The effect of coexisting ions on the adsorption of Sb(III) on γ-Fe_2O_3 magnetic microspheres

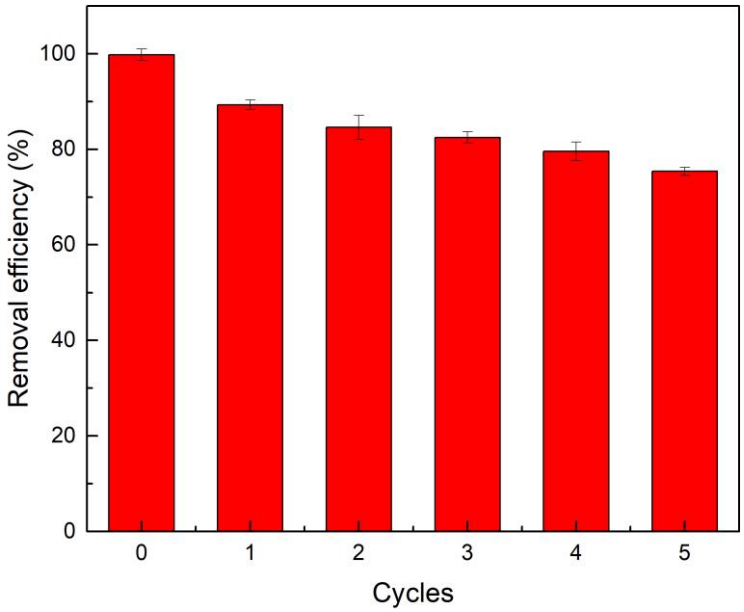

Fig. 15 The reusability of γ-Fe_2O_3 magnetic microspheres for the adsorption of Sb(III)

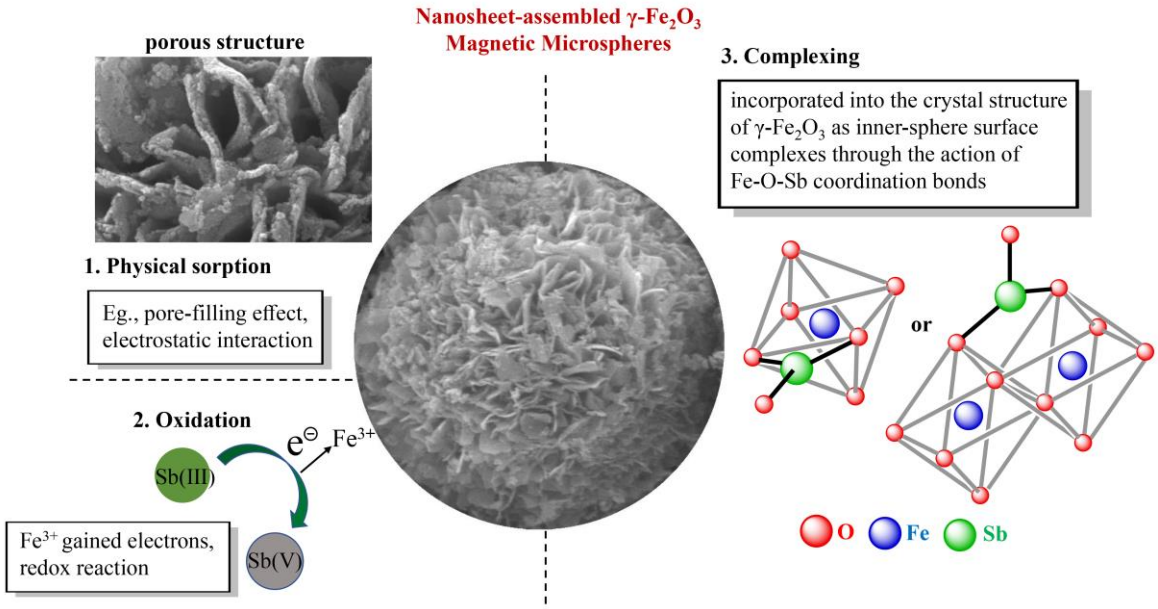

Scheme 1. Speculated enhanced removal mechanisms of Sb(III) by nanosheet-assembled γ-Fe_2O_3 magnetic microspheres